Extreme Mechanics Letters 55 (2022) 101807

Contents lists available at ScienceDirect

Extreme Mechanics Letters

journal homepage: www.elsevier.com/locate/eml

Pulling actuation enabled by harnessing the torsional instability of hyperelastic soft rods

Wei Zhou, Zheng Jia *

State Key Laboratory of Fluid Power and Mechatronic Systems, Key Laboratory of Soft Machines and Smart Devices of Zhejiang Province, Center for X-Mechanics, Department of Engineering Mechanics, Zhejiang University, Hangzhou, 310027, China

ARTICLE INFO

Article history:
Received 29 March 2022
Received in revised form 17 May 2022
Accepted 1 June 2022
Available online 7 June 2022

Keywords:
Torsional instability
Hyperelastic rods
Actuation
Dimensional analysis
Explicit finite element analysis

ABSTRACT

Torsion applied to a slender soft rod can cause the rod to lose its stability and knot — a phenomenon widely referred to as the torsional instability of elastic rods. Previous studies mainly focus on predicting the critical load, at which the torsional instability occurs, and investigating the post-instability deformation of the rod. Thus far, little attention, if any, has been paid to exploiting the torsional instability of hyperelastic soft rods to realize functions such as actuation. In this work, we study the twisting process of hyperelastic soft rods through dimensional analysis and explicit finite element method, and find that the axial pulling force of the soft rod suddenly rises drastically immediately after the torsional instability occurs. Further simulations demonstrate that the sharply increased pulling force can be utilized to achieve a large-stroke pulling actuation. The influence of the rod geometry and material properties of the rod on the actuation forces/strains is also discussed. The results of this work are expected to guide the design of novel actuators based on the torsional instability of hyperelastic soft rods.

1. Introduction

Soft robotics has been widely exploited in a variety of fields from industrial manufacturing to healthcare owing to their excellent flexibility and compliance, which has propelled them to be a thriving technology nowadays [1–4]. Soft actuators are the main and indispensable component of soft robotics, which can realize a wide range of actions and motions, enabling soft robots to interact with external environments and complete complicated tasks [5–10]. Therefore, designing soft actuators with reliable functions plays a crucial role in the development of soft robotic systems. Most soft actuators work by responding to external physical or chemical stimuli [11]. For example, soft actuator systems based on liquid crystal elastomers can achieve different shape morphing modes when triggered by light [12]. Thread-like magnetic robots, which have omnidirectional steering and navigation capabilities, can produce large elastic deflection under the remote control of external magnetic fields [13–15]. Nevertheless, these actuators rely on external physical or chemical stimuli, making them difficult to work in complex unstructured environments. For instance, a light-driven actuator can only operate in unobstructed environments [16]. Furthermore, the range of actuation forces that can be accessed by soft actuators is relatively narrow since they do not use rigid mechanisms such as hinges, gears, or shafts to transmit and amplify forces [17]. In addition, the actuation response of many hydrogel-based actuators depends on the slow diffusion of water in the hydrogel, thereby resulting in low actuating speeds [18,19].

Mechanical instabilities are widely recognized as an adverse effect and often avoided in engineering design since they are generally regarded as mechanical failures. However, it is worth noting that the onset of mechanical instability is often accompanied by sudden and significant changes in geometry or force, which can be used to achieve fast and large actuation [20–23]. To this end, actuators utilizing mechanical instabilities as the actuating principle have been proposed in recent years to address the challenges faced by traditional soft actuators [24]. For instance, by exploiting the buckling of flexible beams, soft robots can generate rapid and large deformation and achieve complex motions using low input energy [17]. Soft fluidic actuators can use small amounts of fluid to generate dramatic changes in shape, volume, and output force via snap-through instability [23]. Moreover, mechanically programmable hydrogel assembly systems can achieve abrupt shape transformations in a reversible manner by performing instability-based transitions between mechanically bistable states [18]. That is, soft actuators that harness mechanical instabilities to realize actuation function can produce large deformation and considerable actuation force at high speed. However, most reported instability-enabled actuators are mainly based on well-known instability modes such as buckling and snap-through

* Corresponding author.
E-mail address: zheng.jia@zju.edu.cn (Z. Jia).

https://doi.org/10.1016/j.eml.2022.101807
2352-4316/

instability, whereas the success of employing less-studied instabilities – such as the torsional instability of soft rods – in actuator design remains rather limited.

The torsion of elastic rods has been observed at various length scales, from anchor cables at the macroscale [25], and skeletal muscles at the micro-scale [26], to DNA double helix at the nanoscale [27]. When cylindrical rods are subjected to sufficiently large torsions, they may lose stability, suddenly deforming into a localized helix pattern, followed by knot formation as the rod is twisted further [28–31]. The phenomenon is known as the torsional instability of elastic rods. Previous research on torsional instability mainly focuses on the theoretical analysis of the critical load that induces the instability, while how to exploit the torsional instability receives little attention. In this work, by combining dimensional analysis and explicit finite element method, we systematically investigate the twisting process of hyperelastic soft rods – including the pre-instability deformation stage, the onset of torsional instability, and the post-instability stage – and study the mechanical response of the twisted rods during the entire process. The results show that the axial force of the soft rod increases suddenly and significantly upon the onset of the torsional instability. More importantly, we demonstrate that large-stroke pulling actuation can be achieved by exploiting the sharp increase in axial force that accompanies the torsional instability. This work brings a new member to the instability-enabled actuator family, i.e., pulling actuators based on the torsional instability of hyperelastic rods.

2. Numerical simulations of the torsion process of hyperelastic soft rods

We employ the commercial finite element package, ABAQUS, to conduct a three-dimensional simulation of the torsion process of hyperelastic soft rods. Dynamic/Explicit solver is chosen to solve the large deformation of the hyperelastic rod during twisting, because it can circumvent the convergence issue due to self-contact behavior of the twisted rod at the post-instability stage. The model of the rod is meshed with explicit, linear, three-dimensional eight-node brick elements (C3D8R), with the number of elements being around 10000–15000. Reduced integration and enhanced hourglass control are adopted to enable the elements to have an enhanced tolerance of distortion. The self-contact module in ABAQUS is utilized to model the self-contact behavior of the rod, with the normal contact behavior set as hard contact and the tangential behavior characterized by a friction coefficient of 0.06. We create two reference points and constrain the motion of the two end surfaces of the rod to the motion of the two reference points, respectively, using coupling constraint of kinematic type, so that torsion can be applied to the rod by setting opposite angular velocity of π rad/s at each reference point, which causes the rod to make one full turn per second. At such rotational speed, the kinetic energy of the rod remains less than 5% of the total internal energy throughout the simulation, so the torsion can be considered quasi-static. Meanwhile, the translational displacement of the two reference points is restricted in all directions to simulate the situation where the end-to-end distance of the rod does not change. The mechanical behavior of the rod is characterized by the Arruda–Boyce model whose model parameters include the shear modulus μ, the limiting network stretch λ, and a parameter D which is related to the initial bulk modulus K_0 by $K_0 = \frac{2}{D}$ [32]. In this work, we take $\mu = 20$ MPa, $\lambda = 1$, and $D = 1 \times 10^{-6}$ MPa^{-1}, unless otherwise noted, to simulate an almost inextensible and incompressible rod. The density of the rod is set to 965 kg/m^3. The mass scaling factor is taken to be 10^{-6} to balance the computation speed and the simulation accuracy.

To reveal the characteristics of the torsional instability of a hyperelastic soft rod, we first simulate the deformation of a rod under torsion with a radius of 2 mm and a length of 100 mm as a representative case. Fig. 1 summarizes the simulation results of the resultant torque and axial force of the rod during rod twisting, as well as the corresponding deformed configurations of the rod. The simulated deformation of the hyperelastic rod under torsion is shown in Fig. 1a. The rod is initially straight and not twisted (Snapshot I). As the twisting progresses, the rod gradually bends after two turns of twist and deforms from its trivial undeflected configuration (Snapshot II) into a continuous helix form (Snapshots III and IV). Thereafter, further twisting causes the rod to lose its stability in the eighth turn, resulting in a transition to a localized helical pattern (Snapshot V), as described by Coyne [30]. The formation of the local helix shown in the snapshot V of Fig. 1a marks the onset of the torsional instability. With further increase in torsion, a localized knot forms and the rod is in the self-contact mode (Snapshot VI). The sequential configurational changes of the twisted rod obtained by the simulation is consistent with the experimental observation made by Thompson and Champney [28].

During the simulation, the resultant torque and axial force of the rod can be monitored on the reference points. Note that the torque and axial force extracted from the reference points on both sides of the rod are almost the same, with slight disparity that can be attributed to the small angular acceleration of the rod, which indicates that the torsion process simulated by the dynamic/explicit solver is indeed quasi-static. To this end, in Fig. 1b we plot the resultant torque and axial force obtained at one reference point as a function of the number of twist turns. The data points on the curves, which are marked by Roman numerals, are corresponding to the configurations shown in Fig. 1a. With the number of twist turns increases, the torque ramps up almost linearly prior to the onset of the torsional instability, followed by a slight drop after the rod loses stability, and eventually rises again after the knotting formation of the rod (Fig. 1b). The reduction in resultant torque can be understood as follows: before the torsional instability sets in, the rod is in the form of a continuous helix (Snapshot IV), and thus twists almost uniformly along the rod; after the rod loses its stability, the torsional deformation becomes concentrated at the localized helix (Snapshot V), with the remaining part of the rod untwisting slightly, thereby resulting in the drop in torque.

As shown in Fig. 1b, the evolution of the axial force exhibits a nonlinear trend. At the beginning of the twisting process, the rod is nearly straight and trivially deflected (Snapshot II). Compared to its undeformed configuration, the contour length of the rod increases slightly due to the incompressibility of the rod — during torsion, the rod needs to reduce its radius but increase the contour length to satisfy the requirement of volume conservation [33]. One notes that the end-to-end length of the rod is fixed, thus the rod is in longitudinal compression during the first two twist turns, which manifests as a compressive axial force, as shown in Fig. 1b. Subsequent twisting bends the rod into a three-dimensional highly-deflected helix configuration (Snapshot III), which tends to reduce the end-to-end length of the rod, thereby giving rise to a tensile axial force of the rod since the end-to-end shortening is prohibited by boundary conditions. Thereafter, the axial force increases gently with increasing twist turns (from Snapshot III to Snapshot V). Intriguingly, after the torsional instability sets in, the formation of the localized helix and knot (Snapshot VI) during the eighth twist turn abruptly straightens the rest part of the rod, and causes a rapid and significant increase of the tensile axial force, with the tensile axial force increasing by a factor of 2.8 in the eighth turn, which constitutes a salient feature of torsional instability. Finally, after the knot formation of

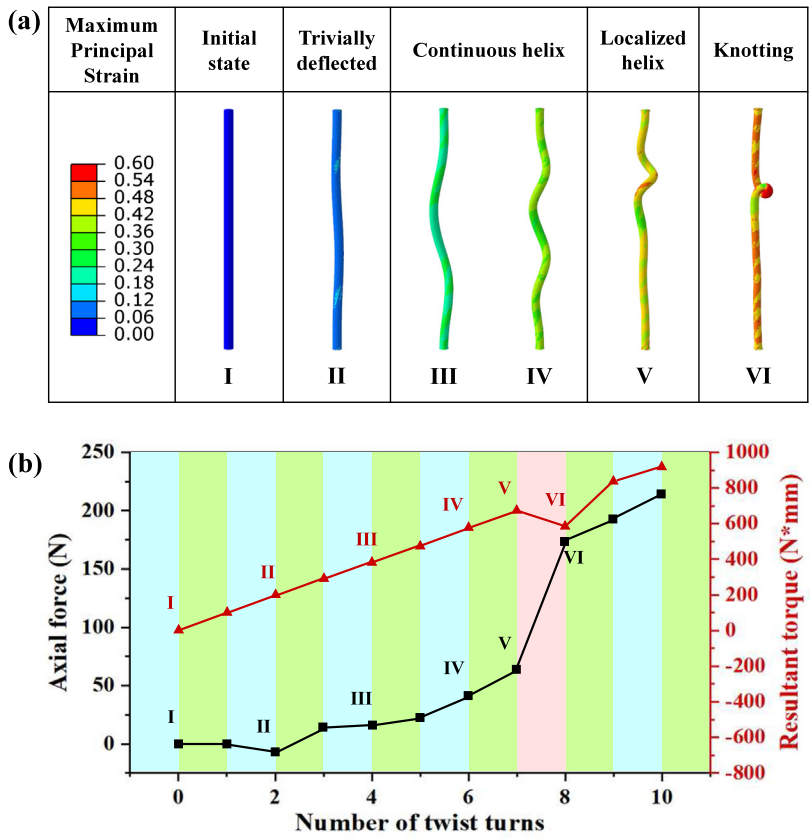

Fig. 1. Simulation results of a representative hyperelastic rod with a radius of 2 mm and a length of 100 mm under torsion. (a) Sequential deformed configurations of the rod during the torsion process. The formation of the localized helix (snapshot V) marks the occurrence of the torsional instability. The color contour represents the maximum principal strain. (b) The resultant torque and axial force plotted as a function of the number of twist turns. The twist turn in which the torsional instability takes place is highlighted by pink. Notably, the occurrence of torsional instability is accompanied by a sharp increase of the axial force as well as a slight drop in the torque.. (For interpretation of the references to color in this figure legend, the reader is referred to the web version of this article.)

the rod, the axial force still keeps rising, but at a much slower rate relative to the increase immediately after the torsional instability begins. The sudden and drastic increase in axial force provides the opportunity to harness the torsional instability of hyperelastic rod to achieve large-stroke pulling actuation. Details on the use of torsional instability to realize pulling actuation will be discussed in later sections.

3. The influence of rod geometry on the mechanical response of twisted hyperelastic rods

In the previous section, the torsion process of a representative hyperelastic rod has been studied. The simulation results suggest that the sharp force increase induced by the torsional instability can be potentially used to achieve pulling actuation. However, the effect of the rod geometry on the mechanical response of the twisted rod remains elusive. In this regard, further simulations on rods of different sizes are subsequently carried out to find the general law governing the torsion process of hyperelastic rods. Dimensional consideration gives the expressions of axial force F and torque T of the rod taking the form

$$F = f\left(\frac{R}{L}, N, \lambda\right)\mu R^2, \tag{1}$$

$$T = t\left(\frac{R}{L}, N, \lambda\right)\mu R^3, \tag{2}$$

where μ and λ are the model parameters of the Arruda–Boyce model, being the shear modulus and the limiting network stretch of the rod material, respectively. R and L denote the radius and length of the rod, N is the number of twist turns. $f\left(\frac{R}{L}, N, \lambda\right) = F/\mu R^2$ and $t\left(\frac{R}{L}, N, \lambda\right) = T/\mu R^3$ are dimensionless functions representing the normalized axial force and normalized torque, respectively, and they depend on three dimensionless parameters, $\frac{R}{L}$, N, and λ. To systematically investigate the size effect on the mechanical response of hyperelastic soft rods under torsion and verify Eqs. (1) and (2), three groups of rods with different radius-to-length ratio R/L are simulated and rods in each group possess the same radius-to-length ratio but different radii and lengths (Table 1).

Fig. 2 plots the normalized axial force $F/\mu R^2$ and normalized torque $T/\mu R^3$ versus the number of the twist turns N. As predicted by Eqs. (1) and (2), it can be observed that for rods of the same radius-to-length ratio R/L, the $F/\mu R^2$ – N curves almost overlap, and so do the $T/\mu R^3$ – N curves. The small differences that manifest as the curve fluctuations can be attributed to numerical errors corresponding to the dynamic effects, due to the dynamic/explicit solver employed in this work. Fig. 2 also shows that rods with larger radius-to-length ratio R/L exhibit higher normalized torque and normalized axial force for the same number of twist turns N, and requires fewer twist turns to trigger torsional instability — the rod with $R/L = 1/50, 1/100, 1/150$ loses stability in the 8th, 13th, and 16th twist turn, respectively. More importantly, after the torsional instability sets in, the axial pulling force of the rod rises sharply until a localized knot is formed on the rod. The axial force that corresponds to the moment of knot formation on the rods can be defined as the limiting pulling force, which can be used to assess the actuation capability of the rod. In this regard, we find that rods with larger radius-to-length ratio R/L possess higher pulling capability. Specifically,

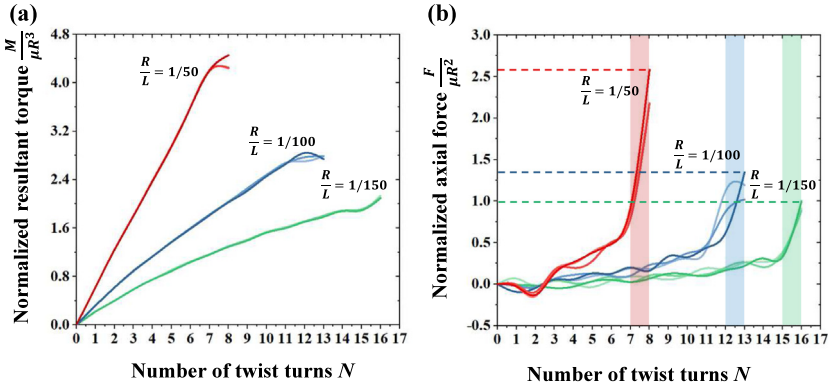

Fig. 2. Mechanical response of hyperelastic rods of different sizes under torsion. (a) The normalized resultant torque of rods under torsion. (b) The normalized axial force of rods under torsion. The curves with the same radius-to-length ratio almost overlap, and the small disparity manifesting as the curve fluctuations can be attributed to numerical errors due to the dynamic/explicit solver.

Table 1
Dimensions of hyperelastic rods simulated.

	R/L	R (mm)	L (mm)
Group 1	1/50	1	50
		2	100
		4	200
Group 2	1/100	1	100
		2	200
		4	400
Group 3	1/150	1	150
		2	300
		4	600

the limiting pulling force is 2.58, 1.37, and 0.98 for radius-to-length ratios of 1/50, 1/100, 1/150, respectively. That is, for hyperelastic rods with the same radius, the shorter the rod, the higher the pulling capability. This provides quantitative guidance for designing the pulling actuators based on torsional instability of hyperelastic rods.

4. Pulling actuators based on the torsional instability of hyperelastic rods

Due to the sharp increase of the axial force associated with the formation of the localized helix and knot, torsional instability can be exploited to achieve pulling actuation. As shown in Fig. 3a, one practical pulling actuator based on this idea is comprised of a hyperelastic soft rod, a stepper motor connected to one end of the soft rod, and a slider that is attached to the other end of the rod whose rotation is inhibited by the track-roller system. When the torque applied by the stepper motor triggers the torsional instability of the rod, that actuator works by displacing the object connected to the slider by virtue of the large axial force of the twisted rod, not relying on any external physical or chemical stimuli. The practical design shown in Fig. 3a can be used to experimentally explore the applications of pulling actuators based on torsional instability of soft rods. However, this work focus on demonstrating the working principle of the pulling actuators by numerical simulation. Thus a simplified model of this actuator is built in ABAQUS as shown in Fig. 3b–d: we simulate a hyperelastic rod with a block of dead weight G attached to the bottom end of the rod. The unattached top end of the rod is fixed and can only rotate along the longitudinal axis of the rod; the rotation of the dead weight is prohibited. The same material properties used in previous simulations are adopted here. Three actuators with the same radius but different lengths are investigated, whose radius-to-length ratio is $R/L = 1/150$ (Fig. 3b), $1/100$ (Fig. 3c), and $1/50$ (Fig. 3d), respectively. The dead weight G is set to $G/\mu R^2 = 1.25$ (Fig. 2b) to test the performance of the pulling actuators. Initially, the block of dead weight is placed on the ground and the rod is straight and unstretched. An angular velocity of 2π rad/s is applied to the top end of the rod.

Assume the torsional instability of a hyperelastic rod occurs in the N^{th} twist turn. The initial configuration and the deformed configurations at the beginning and the end of the N^{th} turn are shown in Fig. 3 to demonstrate the function of the pulling actuators. For a rod with an R/L ratio of 1/150, the torsional instability occurs in the 16th turn and the axial force of the rod increases rapidly as shown in Fig. 2b, however, the axial force upon knot formation is not large enough to pull the dead weight off the ground, since the dead weight of $G/\mu R^2 = 1.25$ exceeds the limiting pulling force of the rod, which is about $F/\mu R^2 = 0.98$ as shown in Fig. 2b. Therefore, the mass is still on the ground at the end of the 16th turn (Fig. 3b). For a rod with an R/L ratio of 1/100, the torsional instability takes place in the 13th turn. In this case, the limiting pulling force of the rod $F/\mu R^2 = 1.37$ is slightly higher than the dead weight of $G/\mu R^2 = 1.25$ (Fig. 2b), thus the block is lifted off the ground at the end of the 13th turn (Fig. 3c). In addition, for a relatively shorter rod with an R/L ratio of 1/50, as the rod loses its stability, a large portion of the rod snarls, accompanied by a rapid increase of axial force rising to $F/\mu R^2 = 2.58$ (Fig. 2b), way beyond the level of the dead weight $G/\mu R^2 = 1.25$, such that the block is lifted away from the ground by a large distance compared to the original length of the rod (Fig. 3d). That is, rods with reasonably higher R/L ratio can successfully lift the mass, realizing pulling actuation, which confirms the feasibility of exploiting torsional instability of hyperelastic rods to design pulling actuators.

To further quantify the performance of the pulling actuators, given a dead weight $G/\mu R^2$, we can define a concept of actuation strain ε_a as

$$\varepsilon_a = H/L, \tag{3}$$

where H represents the height that the mass is pulled off the ground at the end of the N^{th} turn in which torsional instability occurs, and L is the initial length of the rod as mentioned above. Fig. 3e summarizes the actuation strains of the rods with radius-to-length ratio of $R/L = 1/50$, $1/100$, and $1/150$, respectively. The actuation strain increases from 0 for $R/L = 1/150$, to 0.347 for $R/L = 1/100$, and to 0.822 for $R/L = 1/50$, further confirming that rods with higher R/L value exhibiting better actuating performance. Moreover, the rod with $R/L = 1/50$ shows an actuation strain of 0.822, which indicates that the actuator based on torsional instability can achieve large-stroke pulling actuation.

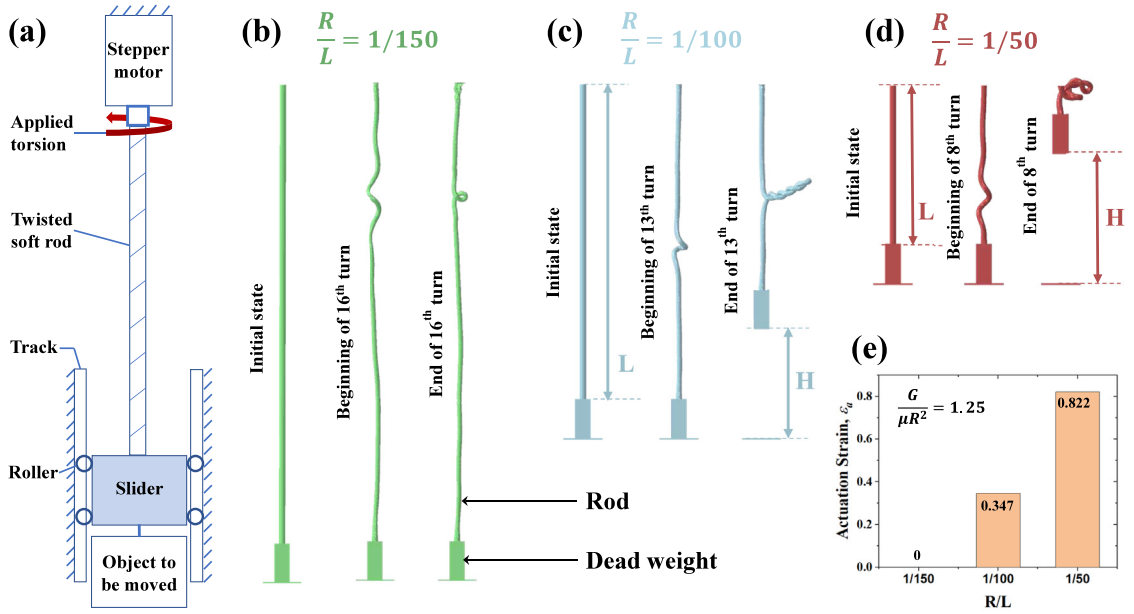

Fig. 3. Pulling actuation enabled by harnessing the torsional instability. (a) One practical design of pulling actuators based on the torsional instability of soft rods. The simplified simulation model of pulling actuators with (b) $R/L = 1/150$, (c) $R/L = 1/100$, and (d) $R/L = 1/50$. It is shown that rods with reasonably large R/L values can successfully lift the load hanging below. (e) The actuation strain of rods with $R/L = 1/150$, $R/L = 1/100$, and $R/L = 1/50$, given a dead weight of $G/\mu R^2 = 1.25$.

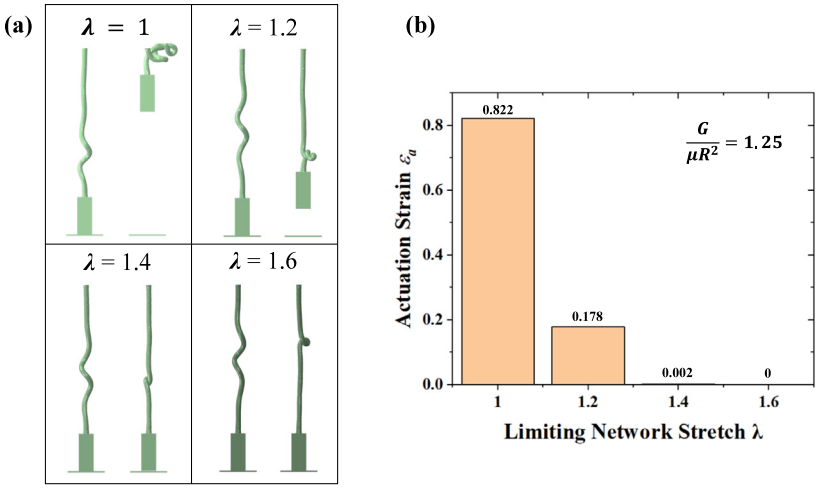

Fig. 4. Effect of the stretchability of the rod on the actuating performance. (a) Performance of the rod with $\lambda = 1$, $\lambda = 1.2$, $\lambda = 1.4$, and $\lambda = 1.6$. The deformed configurations of the rod at the beginning and the end of the twist turns in which torsional instability occurs are shown in the figure. (b) Actuation strains of the four rods given the dead weight $G/\mu R^2 = 1.25$.

Previous simulations have shown that the rod sizes (i.e., the radius-to-length ratio) are critical for the design of the pulling actuator. However, the effect of material properties of the rod, such as stretchability, on the performance of the pulling actuators has not been studied. As a parameter that measures the limiting network stretch of the rod, λ may have a great influence on the torsional instability as well as the actuation performance, but is set to 1 in all previous simulations. To understand the influence of the limiting network stretch λ, we simulate four rods with $\lambda = 1$, 1.2, 1.4 and 1.6, respectively. The radius-to-length ratio is $R/L = 1/50$ and the dead weight is set to $G/\mu R^2 = 1.25$. As shown in Fig. 4a, the rod with $\lambda = 1$ and 1.2 can successfully lift the mass, but with the slight increase of λ, the actuation strains drop significantly from $\varepsilon_a = 0.822$ for $\lambda = 1$ to $\varepsilon_a = 0.178$ for $\lambda = 1.2$. (Fig. 4b). The reason can be understood as follows: a rod with small λ quickly stiffens when being stretched, thus it pulls up the mass hanging below upon the onset of torsional instability rather than being stretched by the mass. In the contrary, the rods with $\lambda = 1.4$ and 1.6 stiffen much more slowly than rods with smaller λ values. As a result, the rods remain soft and can be stretched easily by the dead weight after torsional instability takes place, therefore, the rod with $\lambda = 1.4$ can only lift the mass just off the ground, with a trivial actuation strain being 0.002, and the rod with $\lambda = 1.6$ fails to achieve pulling actuation (Fig. 4a). That is, a rod with lower stretchability exhibits enhanced actuation performance. To this end, the materials such as natural rubber [28], fluoroelastomer rubber, ethylene propylene diene rubber, and nitrile butadiene rubber [33] – they possess limited stretchability and harden quickly upon stretching – can be used to design torsional-instability-based pulling actuators, enabling a great number of potential applications. For example, the soft rods made of these materials can be used in soft robots as artificial muscles, utilizing the actuation force generated by torsional instability to drive the robotic arm to achieve desired motions.

5. Summary

In conclusion, by resorting to finite element simulation with dynamic/explicit solver in ABAQUS, we propose a soft pulling actuator based on the torsional instability of slender hyperelastic rod, by harnessing the sharp increase in axial force when the rod loses stability under torsion. Compared to existing soft actuators that rely on external physical and chemical stimuli such as light, magnetic field and, pH values, the pulling actuator presented in this work can function in response to mechanical torsion, a mechanical stimulus that can be simply applied even in unstructured environment. The pulling actuator can achieve large-stroke pulling actuation with a considerable actuation strain beyond 80% in some specific cases. The actuating force and strain can be adjusted by tuning the dimensions and material properties of the rod. This work paves the way for designing new soft actuators that harness the instability of soft materials.

Declaration of competing interest

The authors declare that they have no known competing financial interests or personal relationships that could have appeared to influence the work reported in this paper.

Acknowledgments

This work is supported by the National Natural Science Foundation of China (Grant Nos. 11802269 and 12072314), Natural Science Foundation of Zhejiang Province, China (Grant No. LR22A020005), and the 111 Project, China (Grant No. B21034).

Appendix A. Supplementary data

Supplementary material related to this article can be found online at https://doi.org/10.1016/j.eml.2022.101807.

References

[1] T. Mirfakhrai, J.D. Madden, R.H. Baughman, Polymer artificial muscles, Mater. Today 10 (4) (2007) 30–38.
[2] F. Rosso, et al., Smart materials as scaffolds for tissue engineering, J. Cell. Physiol. 203 (3) (2005) 465–470.
[3] D. Morales, et al., Electro-actuated hydrogel walkers with dual responsive legs, Soft Matter 10 (9) (2014) 1337–1348.
[4] J.T. Godfrey, Soft Robotic Actuators, University of California, Irvine, 2017.
[5] M. Li, et al., Soft actuators for real-world applications, Nature Rev. Mater. (2021) 1–15.
[6] C. Laschi, et al., Design of a biomimetic robotic octopus arm, Bioinspiration Biomim. 4 (1) (2009) 015006.
[7] F. Ilievski, et al., Soft robotics for chemists, Angew. Chem. 123 (8) (2011) 1930–1935.
[8] B. Mosadegh, et al., Pneumatic networks for soft robotics that actuate rapidly, Adv. Funct. Mater. 24 (15) (2014) 2163–2170.
[9] R.V. Martinez, et al., Robotic tentacles with three-dimensional mobility based on flexible elastomers, Adv. Mater. 25 (2) (2013) 205–212.
[10] R.V. Martinez, et al., Soft actuators and robots that are resistant to mechanical damage, Adv. Funct. Mater. 24 (20) (2014) 3003–3010.
[11] A. Miriyev, K. Stack, H. Lipson, Soft material for soft actuators, Nature Commun. 8 (1) (2017) 1–8.
[12] B. Zuo, et al., Visible and infrared three-wavelength modulated multi-directional actuators, Nature Commun. 10 (1) (2019) 1–11.
[13] R. Zhao, et al., Mechanics of hard-magnetic soft materials, J. Mech. Phys. Solids 124 (2019) 244–263.
[14] Y. Kim, et al., Ferromagnetic soft continuum robots, Science Robotics 4 (33) (2019).
[15] L. Wang, et al., Hard-magnetic elastica, J. Mech. Phys. Solids 142 (2020) 104045.
[16] S. Seok, et al., Meshworm: A peristaltic soft robot with antagonistic nickel titanium coil actuators, IEEE/ASME Trans. Mechatronics 18 (5) (2012) 1485–1497.
[17] A. Pal, et al., Exploiting mechanical instabilities in soft robotics: Control, sensing, and actuation, Adv. Mater. 33 (19) (2021) 2006939.
[18] Q. Zhao, et al., A bioinspired reversible snapping hydrogel assembly, Mater. Horiz. 3 (5) (2016) 422–428.
[19] X. Liu, et al., Hydrogel machines, Mater. Today 36 (2020) 102–124.
[20] S. Singamaneni, V.V. Tsukruk, Buckling instabilities in periodic composite polymeric materials, Soft Matter 6 (22) (2010) 5681–5692.
[21] D. Chen, et al., Stimuli-responsive buckling mechanics of polymer films, J. Polym. Sci. Part B: Polym. Phys. 52 (22) (2014) 1441–1461.
[22] T. Chen, et al., Harnessing bistability for directional propulsion of soft, untethered robots, Proc. Natl. Acad. Sci. 115 (22) (2018) 5698–5702.
[23] J.T. Overvelde, et al., Amplifying the response of soft actuators by harnessing snap-through instabilities, Proc. Natl. Acad. Sci. 112 (35) (2015) 10863–10868.
[24] Y. Chi, et al., Bistable and multistable actuators for soft robots: Structures, materials, and functionalities, Adv. Mater. (2022) 2110384.
[25] M. Podvratnik, Torsional Instability of Elastic Rods, University of Ljubljana, 2011.
[26] C.O. Horgan, J.G. Murphy, The effect of fiber–matrix interaction on the kinking instability arising in the torsion of stretched fibrous biofilaments, J. Mech. Behav. Biomed. Mater. 124 (2021) 104782.
[27] S. Goyal, N. Perkins, C.L. Lee, Torsional buckling and writhing dynamics of elastic cables and DNA, in: International Design Engineering Technical Conferences and Computers and Information in Engineering Conference, 2003.
[28] J. Coyne, Analysis of the formation and elimination of loops in twisted cable, IEEE J. Ocean. Eng. 15 (2) (1990) 72–83.
[29] A. Gent, K.-C. Hua, Torsional instability of stretched rubber cylinders, Int. J. Non-Linear Mech. 39 (3) (2004) 483–489.
[30] J.M.T. Thompson, A. Champneys, From helix to localized writhing in the torsional post-buckling of elastic rods, in: Localization and Solitary Waves in Solid Mechanics, World Scientific, 1999, pp. 111–132.
[31] A.E.H. Love, A Treatise on the Mathematical Theory of Elasticity, Cambridge University Press, 2013.
[32] E.M. Arruda, M.C. Boyce, A three-dimensional constitutive model for the large stretch behavior of rubber elastic materials, J. Mech. Phys. Solids 41 (2) (1993) 389–412.
[33] T. Helps, et al., Twisted rubber variable-stiffness artificial muscles, Soft Robotics 7 (3) (2020) 386–395.